


Rapidly rotating self-gravitating Boussinesq fluid. II. Onset of thermal inertial convection in oblate spheroidal cavities

Wenbo Li 

*State Key Laboratory of Lunar and Planetary Sciences,
Macau University of Science and Technology, Taipa, Macao 999078, China;
CNSA Macau Center for Space Exploration and Science, Macao 999078, China;
and CAS Key Laboratory of Planetary Sciences, Shanghai Astronomical Observatory,
Chinese Academy of Sciences, Shanghai, 200030, China*

Dali Kong *

*CAS Key Laboratory of Planetary Sciences, Shanghai Astronomical Observatory,
Chinese Academy of Sciences, Shanghai, 200030, China*



(Received 9 July 2022; accepted 12 September 2022; published 27 October 2022)

The problem of thermal instability in rapidly rotating, self-gravitating fluid bodies has been widely modeled in spheres or spherical shells, which implicitly neglects the flattening effect due to the centrifugal force. In our previous paper [Kong, *Phys. Rev. Fluids* **7**, 074803 (2022)], by self-consistently taking into account the centrifugal force, rapidly rotating stably stratified Boussinesq fluid was modeled in oblate spheroidal cavities whose geometric shapes are determined by the theory of figure. A closed-form solution was obtained for gravity and temperature. The stable stratification was demonstrated to be motionless in the corotating frame of reference. Based on this nonspherical model of the conduction state in a rapidly rotating spheroidal cavity, the problem of thermal instability is formulated and discussed by this paper in the regime of inertial convection, which is marked by asymptotically small Ekman number and sufficiently small Prandtl number. The critical properties of inertial modes are explicitly derived. The dependence of the onset of thermal inertial convection on the oblateness of spheroid is systematically explored.

DOI: [10.1103/PhysRevFluids.7.103502](https://doi.org/10.1103/PhysRevFluids.7.103502)

I. INTRODUCTION

Convection inside a planet plays an important role in planetary evolution [1,2], chemical mixing [3], and magnetic field generation [4–6]. As generally acknowledged, a planetary fluid layer that possesses enough internal thermal energy could sustain active buoyancy-driven convection, which is usually seen in the interiors of gaseous planets or the liquid layers of terrestrial planets. However, there is no simple global criterion by which one can straightforwardly judge whether or not thermal convection takes place in a planetary interior, especially when the planet is rapidly rotating [7,8].

Chandrasekhar [9] first formulated the problem of thermal instability in rotating fluid spheres and spherical shells under the Boussinesq approximation and the assumption of uniform distribution of heat sources. From then on, much attention has been paid to the role of rotation in altering the onset of rotating Boussinesq convection [8,10–18]. When the Prandtl number of a rotating fluid, which is the ratio of the kinematic viscosity ν to the thermal diffusivity κ , is finite ($0 < \text{Pr} < \infty$), there are several nondimensional numbers that can reflect the relative importance of rotational effects.

*dkong@shao.ac.cn

Denote the angular speed of rotation by Ω , the typical length scale of the fluid layer by d , the typical flow speed by \mathcal{U} , the fluid density by ρ , and the universal gravitational constant by G . Planets are usually called rapidly rotating, because Ekman number $\text{Ek} = \nu/(\Omega d^2)$, which compares viscous force to Coriolis force, is usually asymptotically small at the global scale ($0 < \text{Ek} \ll 1$), and Rossby number $\text{Ro} = \mathcal{U}/(\Omega d)$, which compares inertial force to Coriolis force, is also usually small. One of the good examples is our Earth. In the convective liquid core, the Ekman number is smaller than 10^{-15} [19], the Rossby number can be as small as 10^{-6} [19]. Generally speaking, in the context of geophysical and astrophysical fluid dynamics, extremely small Ekman number and small Rossby number mean that Coriolis force plays a controlling role in thermal instability. This has been extensively justified, for rotating convections [20–27]. Meanwhile, Another rotational parameter, Froude number, being defined as $\text{Fr} = 3\Omega^2/(4\pi G\rho)$, measures the relative strength between centrifugal force and self-gravity. By far, in studies of the problem of thermal instabilities, effects of centrifugal force have been neglected. People believe the much simple spherical problem would give a good approximation to the actual oblate problem. But this has not been rigorously verified by any mathematical or numerical studies. A fundamental scientific question is how centrifugal force would change the onset of thermal instability in a rapidly rotating fluid.

One obvious consequence of the centrifugal force is the nonspherical shape of the fluid domain [28]. For an isolated, uniformly rotating, and self-gravitating Boussinesq fluid of a constant density ρ , to the leading order of the rotational equilibrium, its geometrical figure can be described by a Maclaurin spheroid [29] with equatorial radius R_e and polar radius R_p and hence spheroidal eccentricity $\mathcal{E} = \sqrt{R_e^2 - R_p^2}/R_e$. The eccentricity and the Froude number obey the classical relation

$$\frac{2\text{Fr}}{3} = \frac{\sqrt{1 - \mathcal{E}^2}}{\mathcal{E}^3} (3 - 2\mathcal{E}^2) \sin^{-1} \mathcal{E} - \frac{3(1 - \mathcal{E}^2)}{\mathcal{E}^2}, \quad (1)$$

such that the outer surface is equipotential (the gravitational potential plus the centrifugal potential). Note that, unlike the Maclaurin spheroid solution, the geoid for a rotating, self-gravitating compressible fluid can not be explicitly expressed by any closed-form formulation [30,31]. After all, nonspherical geometry would significantly complicate theoretical or numerical analyses. Most numerical convection models based on finite-difference or spectral methods discretize the governing equations over regular spatial grids in spherical coordinates (r, θ, ϕ) (see compilations of popular codes discussed by Jackson *et al.* [32] and Matsui *et al.* [33]). It is not straightforward to extend them from spherical settings to nonspherical ones because the bounding surface of the domain will not coincide with any particular radial coordinate level surface, which either prevents applying boundary conditions or breaks the condition that can separate radial and angular functions. In principle, finite-element and finite-volume methods that adopt nonstructured meshes are more adaptable to nonspherical geometries, including oblate spheroids [34,35].

Another more intricate effect related to the centrifugal force is a baroclinic state. Von Zeipel in 1924 [36] first derived the condition under which a stably stratified radiative star would rotate uniformly. In order that the stable stratification satisfying the mechanical equilibrium condition can remain hydrostatic in the corotating frame of reference, the internal state of the rotating fluid has to satisfy

$$\varepsilon = C \left(1 - \frac{\Omega^2}{2\pi G\rho} \right), \quad (2)$$

where ε is the rate of heat generation per unit mass, C is a constant. Because the condition suggested by Eq. (2) can hardly be physically sound for stellar interiors [37,38], it is generally found that centrifugal-force-related baroclinicity arises and results in differential rotation, meridional circulation, turbulent mixing, and even dynamo action [39–47]. Note that the rotational baroclinic state is essentially nonhydrostatic and even turbulent in the corotating frame of reference. It implies that if such baroclinicity is a necessary result of the centrifugal force, then the onset of thermal instability is not represented by a Hopf bifurcation, which will cause a fundamental difficulty for analysis.

In our previous paper [48] (hereafter being referred to as K1), however, it was demonstrated by mathematical and numerical examples that the centrifugal-force-related baroclinicity could vanish in the interior of planets, mainly because there was no nuclear fusion process generating energy, hence the assumptions and conditions of the von Zeipel theorem could be exactly satisfied. As a result, in the corotating frame of reference, it is still possible to have a hydrostatic stably stratified conduction state before thermal instability takes place, which provides a crucial basic reference state for perturbation analysis.

Although there are challenges to understanding the effect of centrifugal force in rotating convection, it is scientifically meaningful to make efforts. There are many stellar and planetary objects undergoing extremely fast rotation. Some massive Be-type stars, such as α Arae [49] and α Eridani [50], are famous for their unusual rapidly rotational velocity, causing them to become very oblate. Maeder *et al.* (2008) [51] examined the effects of rotation on the thermal gradient in convective zones of massive stars and discussed the criterion for convection in rotating envelopes. In our Solar System, giant planets such as Jupiter and Saturn are rotating very fast. Their Froude numbers are no longer small and their flattened shapes are apparent. In the era of the Juno and Cassini missions, the measurements of gravitational fields of the two gaseous planets are so accurate that their deep convective motions can be detected via their gravitational signatures [52–55]. Note that the gravitational field of a gaseous planet measured by a spacecraft is always the total one, including both the main field of the nonspherical rotating equilibrium structure and the dynamical distortions resulting from fluid motions. To convincingly separate the dynamical part from the predominant equilibrium background field, it is necessary to self-consistently model the convection [56–58] inside a nonspherical planet, where the centrifugal force is not neglected.

The present work, for the first time, models the onset of thermal instability in significantly flattened spheroids of rapid rotation, by self-consistently taking into account of Coriolis force, centrifugal force, and nonspherical shape. The analysis focuses on the regime of asymptotically small Ekman number and small Prandtl number, but the Froude number is not assumed small. In K1, a nonspherical model of stable stratification was analytically constructed for rapidly rotating Boussinesq fluid of uniform distribution of heat sources. The gravity and temperature solutions were presented as closed-form formulations, in terms of oblate spheroidal coordinates defined in an oblate spheroidal cavity whose geometrical figure shall obey the Maclaurin spheroid relation Eq. (1) rather than arbitrarily chosen. It was mathematically demonstrated that the rotating stable stratification is hydrostatic in the corotating frame of reference, free of baroclinicity because the assumptions and conditions of the von Zeipel theorem can be fully satisfied. The nonspherical model of stable stratification is herein adopted as the conduction state before the onset of thermal instability. By assuming the Ekman number is asymptotically small and the Prandtl number is sufficiently small, linear stability analysis is carried out to determine the critical stratification number and the critical frequency for each particular inertial wave mode in oblate spheroidal cavities of different eccentricity and Froude number. The most unstable modes are numerically verified by three-dimensional finite-element convection models in oblate spheroidal geometries.

In what follows, the hydrostatic basic reference state solution in a Maclaurin spheroid is first discussed in Sec. II. Based on it, the equations to the first order of perturbations, which govern weakly convective motion taking place inside oblate spheroidal cavities, are formulated, subject to no-slip velocity boundary condition and isothermal temperature boundary condition. In Sec. III, under the assumption of an asymptotically small Ekman number and sufficiently small Prandtl number, linear instability analysis is carried out for thermal inertial modes confined in oblate spheroidal cavities, to find the respective critical stratification number for the modes. A global asymptotic solution is derived to describe the criterion for the onset of inertial convection. In Sec. IV, the solution is used to explore how the onset of spheroidal convection depends on the oblateness of the spheroid, or equivalently, on the Froude number. A three-dimensional finite-element method is employed to numerically compute several examples, to verify and validate the theoretical results. Finally, Sec. V summarizes this study and discusses the next works of this paper series.

II. GOVERNING EQUATIONS

Consider a self-gravitating and incompressible Boussinesq fluid confined in an oblate spheroid of eccentricity $0 \leq \mathcal{E} < 1$ with constant thermal diffusivity κ , specific heat capacity at constant pressure c_p , thermal expansion coefficient α , and kinematic viscosity ν . The fluid oblate spheroid rapidly rotating with constant angular velocity $\boldsymbol{\Omega} = \Omega \hat{z}$ is heated internally by a uniform distribution heat sources Q_h per unit volume. When the strength of the heat sources becomes sufficiently strong, the corresponding buoyancy effect would drive convective flow \mathbf{u} and modify the stably stratified thermal profile. The problem of self-consistent convective flow in a rotating oblate spheroid is formulated by the following dimensional equations in the rotating frame [9]:

$$\rho_0 \left(\frac{\partial \mathbf{u}}{\partial t} + \mathbf{u} \cdot \nabla \mathbf{u} + 2\boldsymbol{\Omega} \times \mathbf{u} \right) = -\nabla P + \rho [\mathbf{g}_0 - \boldsymbol{\Omega} \times (\boldsymbol{\Omega} \times \mathbf{r})] + \rho_0 \nu \nabla^2 \mathbf{u}, \quad (3)$$

$$\frac{\partial T}{\partial t} + \mathbf{u} \cdot \nabla T = \kappa \nabla^2 T + \frac{Q_h}{c_p \rho_0}, \quad (4)$$

$$\nabla \cdot \mathbf{u} = 0, \quad (5)$$

$$\nabla \cdot \mathbf{g}_0 = -4\pi G \rho_0, \quad (6)$$

where \mathbf{u} is the fluid velocity relative to the rotating frame, T represents the temperature, P is the hydrodynamic pressure, and ρ_0 is the constant reference density at $T = 0$ and the density obeys $\rho = \rho_0(1 - \alpha T)$, \mathbf{g}_0 is the time-independent gravity, and \mathbf{r} denotes the position vector of fluid parcel. In contrast to previous studies where the effects of centrifugal force associated with density ρ were omitted, the contribution of the centrifugal force is no longer neglected in the further analysis. The equations are defined within the frame of reference attached to a rotating oblate spheroidal cavity whose bounding surface is described in terms of Cartesian coordinates (x, y, z) by

$$S = \left\{ (x, y, z) \left| (x^2 + y^2) + \frac{z^2}{1 - \mathcal{E}^2} = R_e^2 \right. \right\}. \quad (7)$$

The no-slip boundary condition for velocity, the isothermal boundary condition for temperature, and the equipotential equilibrium condition are adopted

$$\mathbf{u}|_S = \mathbf{0}, \quad (8)$$

$$T|_S = 0, \quad (9)$$

$$\left[G \int \frac{\rho_0(\mathbf{r}')}{|\mathbf{r} - \mathbf{r}'|} dV' + \frac{1}{2} |\boldsymbol{\Omega} \times \mathbf{r}|^2 \right]_S = \text{Constant}. \quad (10)$$

The linear properties of weakly convective motion near onset are analyzed through a perturbation approach. Substitution of the expanded solution

$$\mathbf{u} = \mathbf{u}(\mathbf{r}, t), \quad (11)$$

$$T = T_0(\mathbf{r}) + \Theta(\mathbf{r}, t), \quad (12)$$

$$\rho = \rho_0 - \alpha \rho_0 [T_0(\mathbf{r}) + \Theta(\mathbf{r}, t)], \quad (13)$$

$$P = P_0(\mathbf{r}) + p_1(\mathbf{r}, t), \quad (14)$$

into Eqs. (3)–(6) yields the basic state equations for the equilibrium temperature T_0 , density ρ_0 , pressure P_0 , eccentricity \mathcal{E} , and the first-order equations for perturbation variables, velocity \mathbf{u} , temperature Θ , and pressure p .

The equilibrium state is described by the following dimensional equations confined within the spheroidal bounding surface \mathcal{S} ,

$$\rho_0 \boldsymbol{\Omega} \times (\boldsymbol{\Omega} \times \mathbf{r}) = -\nabla P_0(\mathbf{r}) + \rho_0 \mathbf{g}_0(\mathbf{r}), \quad (15)$$

$$\nabla \cdot \mathbf{g}_0(\mathbf{r}) = -4\pi G \rho_0, \quad (16)$$

$$\nabla^2 T_0 + \beta = 0, \quad (17)$$

subject to the the boundary conditions on the spheroidal boundary surface \mathcal{S} ,

$$P_0|_{\mathcal{S}} = \text{Constant}, \quad (18)$$

$$\left[G \int \frac{\rho_0}{|\mathbf{r} - \mathbf{r}'|} dV' + \frac{1}{2} |\boldsymbol{\Omega} \times \mathbf{r}|^2 \right]_{\mathcal{S}} = \text{Constant}, \quad (19)$$

$$T_0|_{\mathcal{S}} = 0, \quad (20)$$

where the positive constant $\beta = Q_h/(c_p \rho_0 \kappa)$. Note that the eccentricity \mathcal{E} of the bounding surface does not explicitly appear in Eqs. (15)–(17). It enters the problem via the equipotential boundary condition Eq. (19). K1 presented the solution to Eqs. (15)–(20) and verified the equilibrium state being exactly hydrostatic. It is convenient to express the solution and conduct further analyses in terms of oblate spheroidal coordinates [59] (η, ϕ, τ) , which can be linked to Cartesian coordinates via

$$x = R_e \sqrt{(\eta^2 + \mathcal{E}^2)(1 - \tau^2)} \cos \phi, \quad (21)$$

$$y = R_e \sqrt{(\eta^2 + \mathcal{E}^2)(1 - \tau^2)} \sin \phi, \quad (22)$$

$$z = R_e \eta \tau, \quad (23)$$

where the z axis is parallel to the angular velocity, $0 \leq \eta \leq \sqrt{1 - \mathcal{E}^2}$ is the radial coordinate, $0 \leq \phi < 2\pi$ is the azimuthal coordinate, and $-1 \leq \tau \leq 1$ is the angular coordinate. According to K1, The solution to Eqs. (15)–(17) subject to boundary conditions Eqs. (18)–(20) on \mathcal{S} where $\eta = \sqrt{1 - \mathcal{E}^2}$ are

$$\hat{\boldsymbol{\eta}} \cdot \mathbf{g}_0 = \gamma R_e \frac{3\eta}{2\mathcal{E}^3} \frac{\sqrt{\eta^2 + \mathcal{E}^2}}{\sqrt{\eta^2 + \mathcal{E}^2 \tau^2}} [\mathcal{E} - 3\mathcal{E}\tau^2 - \mathcal{E}^3(1 - \tau^2) + \sqrt{1 - \mathcal{E}^2}(3\tau^2 - 1) \sin^{-1} \mathcal{E}], \quad (24)$$

$$\hat{\boldsymbol{\tau}} \cdot \mathbf{g}_0 = \gamma R_e \frac{3\tau}{2\mathcal{E}^3} \frac{\sqrt{1 - \tau^2}}{\sqrt{\eta^2 + \mathcal{E}^2 \tau^2}} [-\mathcal{E}^3 + \mathcal{E}^5 + \mathcal{E}(\mathcal{E}^2 - 3)\eta^2 + \sqrt{1 - \mathcal{E}^2}(3\eta^2 + \mathcal{E}^2) \sin^{-1} \mathcal{E}], \quad (25)$$

$$T_0 = \beta R_e^2 \frac{[1 - (\eta^2 + \mathcal{E}^2)][1 - \mathcal{E}^2(1 - \tau^2)]}{6 - 4\mathcal{E}^2}, \quad (26)$$

$$\frac{2\text{Fr}}{3} = \frac{\sqrt{1 - \mathcal{E}^2}}{\mathcal{E}^3} (3 - 2\mathcal{E}^2) \arcsin \mathcal{E} - \frac{3(1 - \mathcal{E}^2)}{\mathcal{E}^2}, \quad (27)$$

where $\gamma = 4\pi G \rho_0/3$. Equation (27) is identical to Eq. (1). Note that our radial coordinate η differs slightly from the ξ defined in K1 by a factor \mathcal{E} . It is then straightforward to find the thermal gradient

$$\hat{\boldsymbol{\eta}} \cdot \nabla T_0 = -\beta R_e \frac{2\eta[1 - \mathcal{E}^2(1 - \tau^2)]}{6 - 4\mathcal{E}^2} \frac{\sqrt{\eta^2 + \mathcal{E}^2}}{\sqrt{\eta^2 + \mathcal{E}^2 \tau^2}}, \quad (28)$$

$$\hat{\boldsymbol{\tau}} \cdot \nabla T_0 = \beta R_e \frac{2\mathcal{E}^2 \tau [1 - (\eta^2 + \mathcal{E}^2)]}{6 - 4\mathcal{E}^2} \frac{\sqrt{1 - \tau^2}}{\sqrt{\eta^2 + \mathcal{E}^2 \tau^2}}. \quad (29)$$

It was demonstrated in K1 that the equilibrium state is free of baroclinicity, which can be quickly shown as the direction of the buoyancy is everywhere parallel to the effective gravity

$$\nabla \times \{T_0[\mathbf{g}_0 - \boldsymbol{\Omega} \times (\boldsymbol{\Omega} \times \mathbf{r})]\} = \nabla T_0 \times [\mathbf{g}_0 - \boldsymbol{\Omega} \times (\boldsymbol{\Omega} \times \mathbf{r})] = \mathbf{0}. \quad (30)$$

Based on the basic conduction state established by Eqs. (24)–(29), the onset of convective motion confined within the spheroidal cavity is governed by the linearized perturbation equations

$$\frac{\partial \mathbf{u}}{\partial t} + 2\boldsymbol{\Omega} \times \mathbf{u} = -\nabla p - \alpha \Theta (\mathbf{g}_0 - \boldsymbol{\Omega} \times \boldsymbol{\Omega} \times \mathbf{r}) + \nu \nabla^2 \mathbf{u}, \quad (31)$$

$$\frac{\partial \Theta}{\partial t} + \mathbf{u} \cdot \nabla T_0 = \kappa \nabla^2 \Theta, \quad (32)$$

$$\nabla \cdot \mathbf{u} = 0, \quad (33)$$

where p is the reduced pressure. Nondimensionalizing Eqs. (31)–(33), by choosing the scalings

$$\mathbf{r} \rightarrow rR_e, \quad t \rightarrow t\Omega^{-1}, \quad p \rightarrow p\rho_0 R_e^2 \Omega^2, \quad \Theta \rightarrow \Theta \beta R_e^2, \quad \text{and } \mathbf{g}_0 \rightarrow \mathbf{g}_0 \gamma R_e, \quad (34)$$

arrives at

$$\frac{\partial \mathbf{u}}{\partial t} + 2\hat{\mathbf{z}} \times \mathbf{u} = -\nabla p + \text{St}(2\text{Fr} - 3)\Theta \nabla T_0 + \text{Ek} \nabla^2 \mathbf{u}, \quad (35)$$

$$\frac{\partial \Theta}{\partial t} + \mathbf{u} \cdot \nabla T_0 = \frac{\text{Ek}}{\text{Pr}} \nabla^2 \Theta, \quad (36)$$

$$\nabla \cdot \mathbf{u} = 0, \quad (37)$$

in which the key dimensionless parameters are defined as

$$\text{St} = \frac{\alpha \beta \gamma R_e^2}{\Omega^2}, \quad \text{Pr} = \frac{\nu}{\kappa}, \quad \text{Ek} = \frac{\nu}{\Omega R_e^2}. \quad (38)$$

When the Froude number Fr and the corresponding eccentricity \mathcal{E} are given, the stratification number St acts a similar role as the Rayleigh number plays in classical formulations of spherical convection problems. But it should be noted that $-\text{St}(2\text{Fr} - 3)$ is the full representation of the strength of unstable stratification. In the spherical limit $\text{Fr} \rightarrow 0$, $\nabla T_0 \rightarrow -\mathbf{r}/3$, it is possible to calculate the equivalent Rayleigh number from a stratification number St . For example, the Rayleigh number defined in Zhang *et al.* (2017) [60] can be calculated as $R = \frac{\alpha \beta \gamma R_e^4}{\Omega \kappa} = \text{St} \times [\text{Pr}/(3\text{Ek})]$. Note that the factor 3 is because they adopted a slightly different definition of β . The equations Eqs. (35)–(37) are equipped with the no-slip velocity and isothermal boundary conditions on $\mathcal{S}(\eta = \sqrt{1 - \mathcal{E}^2})$,

$$\hat{\boldsymbol{\eta}} \cdot \mathbf{u}|_{\mathcal{S}} = \hat{\boldsymbol{\tau}} \cdot \mathbf{u}|_{\mathcal{S}} = \hat{\boldsymbol{\phi}} \cdot \mathbf{u}|_{\mathcal{S}} = \Theta|_{\mathcal{S}} = 0. \quad (39)$$

III. GLOBAL ASYMPTOTIC SOLUTION AND ONSET OF THERMAL INERTIAL WAVE

In classical thermal instability problems in rotating spheres or spherical shells, there are several approaches to determining global onset of convection. One of the most popular idea is looking at the Hopf bifurcation of the eigenproblem resulting from some temporal (e.g., $e^{i\omega t}$) and spatial (e.g., spherical harmonics) decomposition of the governing equations. The eigenfrequency ω is complex. For given values of azimuthal wave number, Ekman number and Prandtl number, the Rayleigh number is increased until the imaginary part of the eigenfrequency decreases from positive to zero signaling the onset of the particular convective mode (e.g., [8,16,61]). The globally most unstable mode can be obtained by minimizing the critical Rayleigh number with respect to the azimuthal wave number.

Another view of the problem is conceptually different. For given values of azimuthal wave number, Ekman number, and Prandtl number, the imaginary part of the eigenfrequency is assumed

to be exactly 0, which means the system must be right at the onset. As a result, Rayleigh number, real-valued eigenfrequency, and convective flow form a definite system that requires some solvability condition being satisfied. This method was first proposed and demonstrated by Zhang and his coauthors since the 1990s [14,15,17,62], and has been applied to various problems (e.g., [60]). The method and relevant examples are comprehensively discussed in a recent text book [63].

We extend the latter idea and the method to obtain the global asymptotic solution of thermal inertial convection in oblate spheroidal cavity valid for $0 < Ek \ll 1$ and sufficiently small Pr subject to no-slip and isothermal boundary conditions. The global asymptotic theory is based on the following hypotheses: (1) a boundary flow in the viscous spheroidal boundary layer must be considered in deriving a global asymptotic solution; (2) the leading-order solution of convection for $0 < Ek \ll 1$ can be represented by a single inertial mode $\mathbf{u}_{mnk}(\eta, \phi, \tau)$ for small Pr.

An asymptotic solution of inertial convection is expanded in the form

$$\mathbf{u} = \mathcal{A}\{[\widehat{\mathbf{u}} + \mathbf{u}_{mnk}(\eta, \phi, \tau)] + \widetilde{\mathbf{u}}\}e^{i2\sigma t} + \text{c.c.} + \dots, \quad (40)$$

$$p = \mathcal{A}\{[\widehat{p} + p_{mnk}(\eta, \phi, \tau)] + \widetilde{p}\}e^{i2\sigma t} + \text{c.c.} + \dots, \quad (41)$$

$$\Theta = \mathcal{A}\Theta_0(\eta, \phi, \tau)e^{i2\sigma t} + \text{c.c.} + \dots, \quad (42)$$

$$\text{St} = \text{St}_1 + \dots, \quad (43)$$

$$\sigma = \sigma_{mnk} + \sigma_1 + \dots, \quad (44)$$

where \mathcal{A} represents the amplitude of convection, \mathbf{u}_{mnk} and p_{mnk} are the primary inertial mode, the boundary flow $\widetilde{\mathbf{u}}$ and the associated pressure \widetilde{p} only exist in the thin boundary layer where $|\widetilde{\mathbf{u}}| = O(|\mathbf{u}_{mnk}|)$, $\widehat{\mathbf{u}}$ and \widehat{p} are the small secondary interior perturbations caused by the boundary flow and vanish in the boundary layer. σ_1 is the small correction to the half eigenfrequency σ_{mnk} of the inertial mode \mathbf{u}_{mnk} , which will be determined with St_1 in the following analysis. c.c. denotes the complex conjugate of the previous term. The order m denotes the azimuthal wave number while k and n represent the radial and axial wave numbers, respectively.

Substitution of Eqs. (40)–(44) into Eqs. (35)–(37) gives rise to the following leading-order problem for a nondissipative inertial wave:

$$i2\sigma_{mnk}\mathbf{u}_{mnk} + 2\hat{\mathbf{z}} \times \mathbf{u}_{mnk} + \nabla p_{mnk} = \mathbf{0}, \quad (45)$$

$$i2\sigma_{mnk}\Theta_0 + \mathbf{u}_{mnk} \cdot \nabla T_0 = \frac{Ek}{Pr} \nabla^2 \Theta_0, \quad (46)$$

$$\nabla \cdot \mathbf{u}_{mnk} = 0, \quad (47)$$

subject to the inviscid, nonpenetrable, and isothermal boundary conditions at $\eta = \sqrt{1 - \mathcal{E}^2}$,

$$\hat{\boldsymbol{\eta}} \cdot \mathbf{u}_{mnk}|_S = \Theta_0|_S = 0, \quad (48)$$

where the imaginary unit $i = \sqrt{-1}$. The Ekman number and Prandtl number do not appear in Eqs. (45) and (47) and only affect the solution Θ_0 in Eq. (46). Zhang *et al.* (2004) [59] first solved Eq. (45) and Eq. (47) in oblate spheroidal geometry. The pressure p_{mnk} is expressed as

$$p_{mnk} = \sum_{i=0}^k \sum_{j=0}^{k-i} C_{mki}^s \sigma_{mnk}^{2i} (1 - \sigma_{mnk}^2)^j [(\eta^2 + \mathcal{E}^2)(1 - \tau^2)]^{m/2+j} (\eta\tau)^{2i} e^{im\phi}, \quad (49)$$

where the coefficient C_{mki}^s is defined as

$$C_{mki}^s = \left[\frac{-1}{(1 - \sigma_{mnk}^2 \mathcal{E}^2)} \right]^{i+j} \frac{[2(m+k+i+j)-1]!!}{2^{j+1}(2i-1)!!(k-i-j)!i!j!(m+j)!}, \quad (50)$$

and the half eigenfrequency σ_{mnk} can be solved from the transcendental equation,

$$0 = m + \sum_{j=0}^{k-1} (-1)^{j+k} \left\{ \frac{k![2(2k+m-j)]!(k+m)!}{[2(k-j)]![2(k+m)]!j!(2k+m-j)!} \right\} \\ \times \left[m - \frac{2(1-\sigma_{mnk})(k-j)}{\sigma_{mnk}(1-\mathcal{E}^2)} \right] \left[\frac{(1-\mathcal{E}^2)\sigma_{mnk}^2}{(1-\sigma_{mnk}^2\mathcal{E}^2)} \right]^{k-j}, \quad (51)$$

with $m \geq 1$ and $k \geq 1$. For a given \mathcal{E} , m , and k , there exist $2k$ different real solutions for σ_{mnk} corresponding to $2k$ different inertial modes which can be arranged according to the size of σ_{mnk} , $0 < |\sigma_{m1k}| < |\sigma_{m2k}| < |\sigma_{m3k}| < \dots < |\sigma_{mnk}| < \dots < 1$, with the σ_{mnk} representing the n th smallest absolute root of Eq. (51). Closed-form velocity components of inertial modes \mathbf{u}_{mnk} can be found in Zhang and Liao (2017) [63]. The order m denotes the azimuthal wave number while n and k , respectively, outline the complexity of the flow structure in the directions perpendicular to and parallel with the rotation axis.

While the inviscid spheroidal inertial modes are given, the temperature Θ_0 , a solution to Eq. (46) subject to isothermal boundary condition, can be derived by virtue of an expansion using the radial spheroidal wave functions of the first kind $R_{ml}^{(1)}(-i\mathcal{E}k_{lq}, i\eta/\mathcal{E})$ and the spheroidal angular functions $S_{ml}^{(1)}(-i\mathcal{E}k_{lq}, \tau)$ of the first kind, which are eigenfunctions of the Helmholtz equation $\nabla^2\psi + k^2\psi = 0$ in oblate spheroidal domain [64,65], in the form

$$\Theta_0 = \sum_{l,q} \Theta_{lq} R_{ml}^{(1)}(-i\mathcal{E}k_{lq}, i\eta/\mathcal{E}) S_{ml}^{(1)}(-i\mathcal{E}k_{lq}, \tau) e^{im\phi}, \quad (52)$$

where Θ_{lq} are the complex coefficients and k_{lq} are determined by zeros of $R_{ml}^{(1)}$ functions,

$$R_{ml}^{(1)}(-i\mathcal{E}k_{lq}, i\sqrt{1-\mathcal{E}^2}/\mathcal{E}) = 0, \quad (53)$$

with k_{lq} being ordered such that $0 < k_{l1} < k_{l2} < k_{l3} < \dots$. The expansion coefficients Θ_{lq} can be figured out,

$$\Theta_{lq} = -\frac{2\pi e^{-im\phi}}{k_{lq}^2 \text{Ek}/\text{Pr} + i2\sigma_{mnk}} \int_{-1}^1 \int_0^{\sqrt{1-\mathcal{E}^2}} (\mathbf{u}_{mnk} \cdot \nabla T_0) R_{ml}^{(1)}(-i\mathcal{E}k_{lq}, i\eta/\mathcal{E}) \\ \times S_{ml}^{(1)}(-i\mathcal{E}k_{lq}, \tau) (\eta^2 + \mathcal{E}^2\tau^2) d\eta d\tau. \quad (54)$$

The spheroidal wave functions $R_{ml}^{(1)}(-i\mathcal{E}k_{lq}, i\eta/\mathcal{E})$ and $S_{ml}^{(1)}(-i\mathcal{E}k_{lq}, \tau)$ have been normalized such that

$$\int_0^{2\pi} \int_{-1}^1 \int_0^{\sqrt{1-\mathcal{E}^2}} R_{ml}^{(1)}(-i\mathcal{E}k_{lq}, i\eta/\mathcal{E}) S_{ml}^{(1)}(-i\mathcal{E}k_{lq}, \tau) \\ \times R_{m'l'}^{(1)}(-i\mathcal{E}k_{l'q'}, i\eta/\mathcal{E}) S_{m'l'}^{(1)}(-i\mathcal{E}k_{l'q'}, \tau) (\eta^2 + \mathcal{E}^2\tau^2) d\eta d\tau d\phi = \delta_{ll'} \delta_{qq'}, \quad (55)$$

where $\delta_{ll'}$ is the Kronecker δ function and $l-m=0, 2, 4, \dots, q=1, 2, 3, \dots$ for an equatorially symmetric mode while $l-m=1, 3, 5, \dots, q=1, 2, 3, \dots$ for an equatorially antisymmetric mode. In practical computations, usually a small number of terms in Eq. (54) are required in the expansion to achieve a reasonable accuracy. For the cases later presented in this paper, the chosen truncation of the expansion is q up to 5 and l up to $m+5$, which has been tested for convergence.

At the next order, the governing equations for the secondary flow $\hat{\mathbf{u}}$ in the interior of the oblate spheroid are,

$$i2\sigma_{mnk}\hat{\mathbf{u}} + 2\hat{\mathbf{z}} \times \hat{\mathbf{u}} + \nabla\hat{p} = \text{St}_1(2\text{Fr} - 3)\Theta_0\nabla T_0 + \text{Ek}\nabla^2\mathbf{u}_{mnk} - i2\sigma_1\mathbf{u}_{mnk}, \quad (56)$$

$$\nabla \cdot \hat{\mathbf{u}} = 0, \quad (57)$$

where higher terms, such as $i2\sigma_1\widehat{\mathbf{u}}$ and $\text{Ek}\nabla\widehat{\mathbf{u}}$, are neglected and the secondary flow $\widehat{\mathbf{u}}$ is subject to the boundary condition,

$$\widehat{\boldsymbol{\eta}} \cdot \widehat{\mathbf{u}} = \text{influx at the outer edge of the viscous boundary layer } \widetilde{\mathbf{u}}. \quad (58)$$

At this order, thermal effects are coupled with the nondissipative thermal-inertial oscillation, driving convection against viscous dissipation. Multiplying Eq. (56) by \mathbf{u}_{mnk}^* , the complex conjugate of \mathbf{u}_{mnk} , and integrating over the oblate spheroid \mathcal{V} gives rise to the solvability condition for the inhomogeneous system Eqs. (56) and (57),

$$\int_S p_{mnk}^* \widehat{\mathbf{u}} \cdot \widehat{\boldsymbol{\eta}} dS = \text{St}_1(2\text{Fr} - 3) \int_{\mathcal{V}} (\mathbf{u}_{mnk}^* \cdot \nabla T_0) \Theta_0 d\mathcal{V} - i2\sigma_1 \int_{\mathcal{V}} |\mathbf{u}_{mnk}|^2 d\mathcal{V}, \quad (59)$$

given the following properties,

$$\int_{\mathcal{V}} \mathbf{u}_{mnk}^* \cdot (i2\sigma_{mnk}\widehat{\mathbf{u}} + 2\widehat{\mathbf{z}} \times \widehat{\mathbf{u}} + \nabla\widehat{p}) d\mathcal{V} = \int_S p_{mnk}^* \widehat{\mathbf{u}} \cdot \widehat{\boldsymbol{\eta}} dS, \quad (60)$$

$$\int_{\mathcal{V}} \mathbf{u}_{mnk}^* \cdot \nabla^2 \mathbf{u}_{mnk} d\mathcal{V} = 0, \quad (61)$$

where p_{mnk}^* is the complex conjugate of p_{mnk} and the viscous integral Eq. (61) has been proved by Zhang *et al.* (2004) [59]. Now the major task is to evaluate the surface integral on the left-hand side of Eq. (59), though the right-hand side can be calculated easily. According to Eq. (58), the explicit expression of the boundary flow $\widehat{\mathbf{u}}$ is needed for the task, which is discussed and derived in the Appendix. Upon recognizing that, in Eq. (A18), the γ_{mnk}^- terms make the same contribution as the γ_{mnk}^+ terms, the surface integral can be computed

$$\begin{aligned} \int_S p_{mnk}^* \widehat{\mathbf{u}} \cdot \widehat{\boldsymbol{\eta}} dS &= i2\pi\sqrt{\text{Ek}} \int_{-1}^1 \frac{V_{mnk}^\tau + V_{mnk}^\phi}{\gamma_{mnk}^+} \\ &\times \left(h\sqrt{1-\tau^2} \frac{dP_{mnk}}{d\tau} + \frac{mh^2}{\sqrt{1-\tau^2}} P_{mnk} \right) d\tau, \end{aligned} \quad (62)$$

in which the symbols V_{mnk}^τ , V_{mnk}^ϕ , P_{mnk} , and h are also introduced in the Appendix.

Substitution of Eq. (62) into Eq. (59) gives rise to the final solvability condition, whose real part can be used to determine the stratification number St_1 ,

$$\begin{aligned} \sqrt{\text{Ek}} \int_{-1}^1 \frac{\sigma_{mnk}h^2 + \tau h}{|\sigma_{mnk}h^2 + \tau h|^{3/2}} (V_{mnk}^\tau + V_{mnk}^\phi) \left(h\sqrt{1-\tau^2} \frac{dP_{mnk}}{d\tau} + \frac{mh^2}{\sqrt{1-\tau^2}} P_{mnk} \right) d\tau \\ = 2\text{St}_1(3 - 2\text{Fr}) \text{Re} \left[\int_{-1}^1 \int_0^{\sqrt{1-\mathcal{E}^2}} (\mathbf{u}_{mnk}^* \cdot \nabla T_0) \Theta_0 (\eta^2 + \mathcal{E}^2\tau^2) d\eta d\tau \right], \end{aligned} \quad (63)$$

while the imaginary part can be used to determine σ_1 , which gives the half frequency via Eq. (44),

$$\begin{aligned} \sqrt{\text{Ek}} \int_{-1}^1 \frac{V_{mnk}^\tau + V_{mnk}^\phi}{|\sigma_{mnk}h^2 + \tau h|^{1/2}} \left(h\sqrt{1-\tau^2} \frac{dP_{mnk}}{d\tau} + \frac{mh^2}{\sqrt{1-\tau^2}} P_{mnk} \right) d\tau \\ = 2\text{St}_1(3 - 2\text{Fr}) \text{Im} \left[\int_{-1}^1 \int_0^{\sqrt{1-\mathcal{E}^2}} (\mathbf{u}_{mnk}^* \cdot \nabla T_0) \Theta_0 (\eta^2 + \mathcal{E}^2\tau^2) d\eta d\tau \right] \\ + 4\sigma_1 \int_{-1}^1 \int_0^{\sqrt{1-\mathcal{E}^2}} |\mathbf{u}_{mnk}|^2 (\eta^2 + \mathcal{E}^2\tau^2) d\eta d\tau, \end{aligned} \quad (64)$$

where the integrals involving Θ_0 can be computed via

$$\begin{aligned} & \operatorname{Re} \left[\int_{-1}^1 \int_0^{\sqrt{1-\mathcal{E}^2}} (\mathbf{u}_{mnk}^* \cdot \nabla T_0) \Theta_0(\eta^2 + \mathcal{E}^2 \tau^2) d\eta d\tau \right] \\ &= - \sum_{l,q} \frac{2\pi k_{lq}^2 \operatorname{Ek}/\operatorname{Pr}}{(k_{lq}^2 \operatorname{Ek}/\operatorname{Pr})^2 + 4\sigma_{mnk}^2} \\ & \quad \times \left| \int_{-1}^1 \int_0^{\sqrt{1-\mathcal{E}^2}} (\mathbf{u}_{mnk} \cdot \nabla T_0) R_{ml}^{(1)}(-i\mathcal{E}k_{lq}, i\eta/\mathcal{E}) S_{ml}^{(1)}(-i\mathcal{E}k_{lq}, \tau)(\eta^2 + \mathcal{E}^2 \tau^2) d\eta d\tau \right|^2, \end{aligned} \quad (65)$$

and

$$\begin{aligned} & \operatorname{Im} \left[\int_{-1}^1 \int_0^{\sqrt{1-\mathcal{E}^2}} (\mathbf{u}_{mnk}^* \cdot \nabla T_0) \Theta_0(\eta^2 + \mathcal{E}^2 \tau^2) d\eta d\tau \right] \\ &= \sum_{l,q} \frac{4\pi \sigma_{mnk}}{(k_{lq}^2 \operatorname{Ek}/\operatorname{Pr})^2 + 4\sigma_{mnk}^2} \\ & \quad \times \left| \int_{-1}^1 \int_0^{\sqrt{1-\mathcal{E}^2}} (\mathbf{u}_{mnk} \cdot \nabla T_0) R_{ml}^{(1)}(-i\mathcal{E}k_{lq}, i\eta/\mathcal{E}) S_{ml}^{(1)}(-i\mathcal{E}k_{lq}, \tau)(\eta^2 + \mathcal{E}^2 \tau^2) d\eta d\tau \right|^2, \end{aligned} \quad (66)$$

and the integral linked to the normalization of an inertial mode \mathbf{u}_{mnk} is given by

$$\begin{aligned} & \int_{-1}^1 \int_0^{\sqrt{1-\mathcal{E}^2}} |\mathbf{u}_{mnk}|^2 (\eta^2 + \mathcal{E}^2 \tau^2) d\eta d\tau \\ &= \sum_{i=0}^k \sum_{j=0}^{k-i} \sum_{\mu=0}^k \sum_{\nu=0}^{k-\mu} \mathcal{C}_{mki}^s \mathcal{C}_{mk\mu\nu}^s \sigma_{mnk}^{2i+2\mu} (1 - \sigma_{mnk}^2)^{j+\nu} \left[\frac{2^{m+j+\nu-2} (1 - \mathcal{E}^2)^{i+\mu+1/2}}{(2m+2i+2j+2\mu+2\nu+1)!!} \right] \\ & \quad \times \left[\frac{\mathcal{H}(m+j+\nu-1)!(2i+2\mu-1)!!}{(1-\sigma^2)^2} + \frac{8i\mu(m+j+\nu)!(2i+2\mu-3)!!}{\sigma^2(1-\mathcal{E}^2)} \right], \end{aligned} \quad (67)$$

with

$$\mathcal{H} = (2j\sigma_{mnk} + m\sigma_{mnk} + m)(2\nu\sigma_{mnk} + m\sigma_{mnk} + m) + (2j + m + m\sigma_{mnk})(2\nu + m + m\sigma_{mnk}),$$

for the nonaxisymmetric and equatorially symmetric mode.

For any given Ekman number Ek that is asymptotically small, Prandtl number Pr that is sufficiently small, and Froude number Fr that obeys the Maclaurin spheroid relation, the globally minimum critical stratification number St_c is determined by minimizing St_1 in Eq. (63) over different inertial modes \mathbf{u}_{mnk} , giving rise to the most unstable mode $\mathbf{u}_{m_c n_c k_c}$ marked by the critical wave numbers $m = m_c$, $n = n_c$ and $k = k_c$ along with the corresponding half eigenfrequency $\sigma_{m_c n_c k_c}$. After the determination of St_1 and the critical inertial mode $\mathbf{u}_{m_c n_c k_c}$, the critical half frequency can be computed by Eq. (64), $\sigma_c = \sigma_{m_c n_c k_c} + \sigma_1$. Finally, the leading order velocity \mathbf{u} of inertial convection in rotating oblate spheroid can be expressed as

$$\mathbf{u} = [\mathbf{u}_{m_c n_c k_c}(\eta, \tau, \phi) + \tilde{\mathbf{u}}_{\text{tang}}] e^{i2\sigma_{m_c n_c k_c} t} + \text{c.c.}, \quad (68)$$

where $\tilde{\mathbf{u}}_{\text{tang}}$ is given by Eqs. (A9)–(A11). The velocity \mathbf{u} of inertial convection not only satisfies the no-slip condition on the spheroidal bounding surface but also is fully analytical in closed form. Equations (63)–(67) describe a complete global asymptotic solution for inertial convection in rapidly rotating oblate spheroids with the no-slip boundary condition. The determination of the small amplitude \mathcal{A} in Eq. (40) needs a higher-order analysis, which is out of the scope of the current research.

In the limit of $Fr \rightarrow 0$, the effects of centrifugal force diminish and hence the oblateness of spheroid $\mathcal{E} \rightarrow 0$, the spheroidal coordinates return to the spherical coordinates $\eta \rightarrow r$, $\tau \rightarrow \cos \theta$. It can be straightforwardly verified that $h = 1$, $\nabla T_0 = -\mathbf{r}/3$ and the spheroidal wave functions $R_{ml}^{(1)}(-i\mathcal{E}k_{lq}, i\eta/\mathcal{E})$ and $S_{ml}^{(1)}(-i\mathcal{E}k_{lq}, \tau)$, respectively, degenerate to spherical Bessel function $j_l(k_{lq}r)$ of the first kind and associated Legendre polynomial $P_l^m(\cos \theta)$. Without surprise, our asymptotic solution Eqs. (63)–(67) will also tend to its spherical limit that has been thoroughly discussed in Chapter 19 of Zhang and Liao (2017) [63].

In this paper, we have focused on the small Prandtl number regime of convection. Under this circumstance, the primary convective flow is nondissipative. As a result, in the leading order problem Eqs. (45)–(47), the temperature Θ_0 a passive variable, implying $St_0 = 0$. The buoyancy term is small and only active in the next order problem Eqs. (56) and (57), driving thermal convection against viscous dissipation in boundary layer. However, if Prandtl number gets larger, or more precisely speaking Pr/Ek becoming large, dynamics enter a different regime. Multiple inertial modes are excited at the onset of convection. Internal viscous dissipation gradually becomes a leading role [16,18,62]. The buoyancy term is no longer small. The overall formulation of the problem of thermal instabilities must be different from Eqs. (40)–(44). The so-called viscous convection problem in oblate spheroidal cavities will be discussed in our future paper.

IV. ANALYTICAL AND NUMERICAL RESULTS

With the global asymptotic solution of inertial convection in rapidly rotating oblate spheroidal cavity, it becomes possible to systematically study the topological properties of onset of convection. It is not our primary purpose in this paper to extensively explore a wide parameter space of Ek , Pr , and Fr . Instead, we focus on some typical examples to demonstrate and validate the obtained solution. In all the results displayed in this section, the Ekman number is fixed at $Ek = 10^{-4}$, which is asymptotically small and meanwhile practical for independent numerical verifications.

Figure 1 shows the onset of several thermal inertial modes, as the function of Prandtl number. Two spheroids of $\mathcal{E} = 0.0818$ and $\mathcal{E} = 0.3543$ are chosen for the purpose of illustration, respectively corresponding to the rotational flattening of Earth and Jupiter. The two cases, displayed in Figs. 1(b) and 1(c), are compared with Fig. 1(a) that plots the result of the classical spherical convection problem where the geometrical and topological effects of the centrifugal force are totally neglected from the dynamics [15,63]. All panels show, when the Prandtl number varies, the globally most unstable mode could change among different ones.

The next figure brings a better view of how the critical stratification numbers and the half eigenfrequencies of the modes depend on the eccentricity of spheroid. Figure 2(a) shows that the critical stratification numbers for all modes rise substantially with the increase of geometrical oblateness. Figure 2(b) demonstrates that, as the eccentricity of the spheroidal cavity is getting larger, the half-frequencies are driven higher for retrogradely propagating modes but largely maintain level for the progradely propagating waves.

Specifically, we pick up a particular Prandtl number $Pr = 5 \times 10^{-3}$ and calculate the asymptotic solutions for the globally critical modes in the three oblate spheroids. The results are listed in Table I.

Following the analytically computed results, the tabulated cases in Table I are also independently calculated by a 3D finite-element method, solving the full nonlinear convection equations,

$$\frac{\partial \mathbf{u}}{\partial t} + \mathbf{u} \cdot \nabla \mathbf{u} + 2\hat{\mathbf{z}} \times \mathbf{u} = -\nabla p + St[Fr\hat{\mathbf{z}} \times (\hat{\mathbf{z}} \times \mathbf{r}) - \mathbf{g}_0]\Theta + Ek\nabla^2 \mathbf{u}, \quad (69)$$

$$\frac{\partial \Theta}{\partial t} + \mathbf{u} \cdot \nabla (T_0 + \Theta) = \frac{Ek}{Pr} \nabla^2 \Theta, \quad (70)$$

$$\nabla \cdot \mathbf{u} = 0, \quad (71)$$

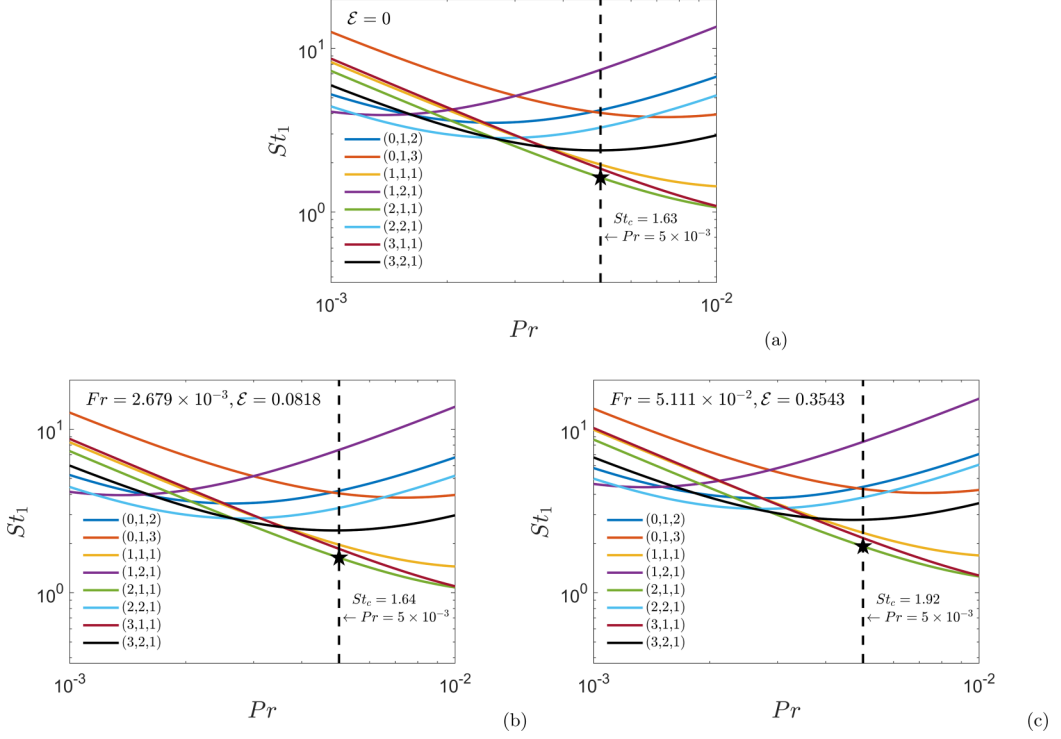


FIG. 1. The onset of several thermal inertial wave modes in oblate spheroidal cavities plotted as functions of the Prandtl number. The critical stratification number St_1 of each mode is plotted in a respective solid curve. The modes are distinguished by different colors and denoted by their azimuthal, axial and radial wave numbers (m, n, k) . The Ekman number is commonly fixed at $Ek = 10^{-4}$. The Prandtl number ranges in $10^{-3} \leq Pr \leq 10^{-2}$. Panel (a) plots the classical spherical convection problem where the centrifugal force is neglected. In this circumstance, the stratification number St can be equivalently converted to the modified Rayleigh number \tilde{Ra} defined by Zhang and Liao (2017) [63] as $\tilde{Ra} = St[Pr/(3Ek)]$. Panels (b) and (c) present results for convections in oblate spheroidal cavities of different rotation rate and hence different eccentricity. In panel (b), $\mathcal{E} = 0.0818$ is chosen to be Earth's oblateness; in panel (c), $\mathcal{E} = 0.3543$ marks a shape that is close to Jupiter. In all panels, the dashed vertical lines select the location of $Pr = 5 \times 10^{-3}$, at which the (2,1,1) modes are always the most unstable. The corresponding global critical stratification numbers St_c are marked by pentacles. With the increase of eccentricity, the St_c value rises.

TABLE I. Two examples of the globally most unstable modes and their critical properties at $Ek = 10^{-4}$ and $Pr = 5 \times 10^{-3}$ in oblate spheroids, obtained with the asymptotic solution. $\sigma_{m_c n_c k_c}$ is the half eigenfrequency of the most unstable inertial mode. $\sigma_c = \sigma_{m_c n_c k_c} + \sigma_1$ is the modified half frequency of the asymptotic solution. The spheroidal geometries are consistent with what are used in Figs. 1(b) and 1(c). Note that the first row presents the critical parameters for the case under spherical approximation. Froude number hence is not part of the model. In this case, the critical stratification number is equivalent to the critical Rayleigh number $Ra_c = St_c[Pr/(3Ek)] = 27.09$.

Ek	Pr	Fr	\mathcal{E}	(m_c, n_c, k_c)	St_c	σ_c	$\sigma_{m_c n_c k_c}$
10^{-4}	5×10^{-3}	—	0	(2,1,1)	1.6253	-0.1096	-0.1160
		2.6791×10^{-3}	0.0818	(2,1,1)	1.6379	-0.1096	-0.1160
		5.1108×10^{-2}	0.3543	(2,1,1)	1.9215	-0.1106	-0.1170

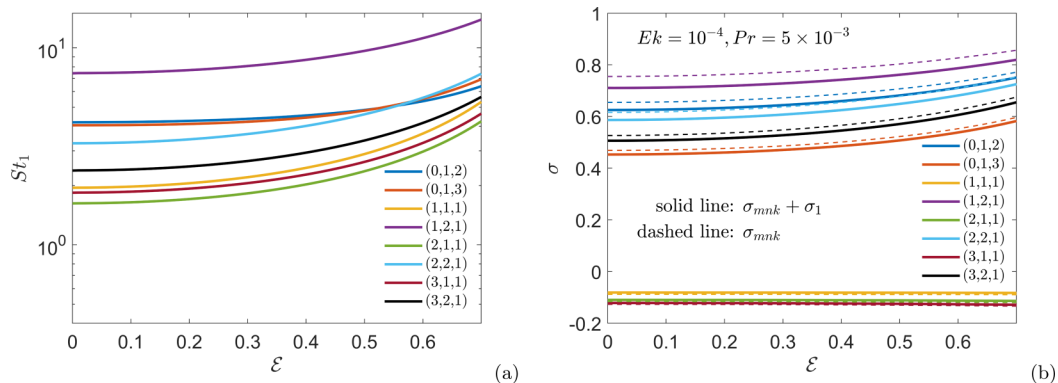


FIG. 2. The onset of several inertial modes in oblate spheroidal cavities as functions of the oblateness of the geometry. The modes are distinguished by different colors and denoted by their azimuthal, axial and radial wave numbers (m, n, k) . The Ekman number and the Prandtl number are commonly fixed at $Ek = 10^{-4}$ and $Pr = 5 \times 10^{-3}$, respectively.

which are numerically computed in an oblate spheroidal geometry,

$$\mathcal{D} = \left\{ (x, y, z) \left| x^2 + y^2 + \frac{z^2}{1 - \mathcal{E}^2} \leq 1 \right. \right\},$$

constructed by an unstructured tetrahedral mesh, as illustrated in Fig. 3.

No-slip and isothermal boundary conditions remain on the bounding surface $\mathcal{S}(\eta = \sqrt{1 - \mathcal{E}^2})$,

$$\mathbf{u}|_{\mathcal{S}} = \mathbf{0}, \quad \Theta|_{\mathcal{S}} = 0.$$

A P2/P1 mixed finite-element scheme is applied to the spatial discretization of the nonlinear partial differential equations [66], while a BDF(2) time stepping scheme is adopted for the temporal discretization [67]. The velocity field \mathbf{u} and the temperature field Θ are expanded into piecewise second-order polynomials by nodal quadratic bases defined on tetrahedral vertices and edge mid-points, while the pressure field p is approximated by a piecewise first-order function constructed by nodal linear bases defined on tetrahedral vertices. A saddle-point algebraic problem is yielded after the Galerkin weighted residual approach is applied [68]. A stabilized Krylov subspace iterative solver (the stabilized BiCG) is used to tackle the system of linear equations [69]. The overall code

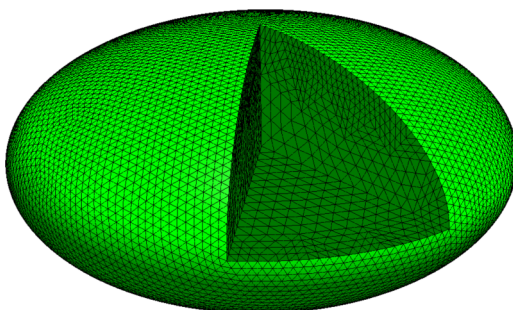


FIG. 3. Sketch of a three-dimensional oblate spheroidal mesh consisting of tetrahedral elements. The mesh is illustrated as being refined near its bounding surface to accurately compute the boundary layer flow. Note that the meshes used in real numerical computations are much denser than this illustration.

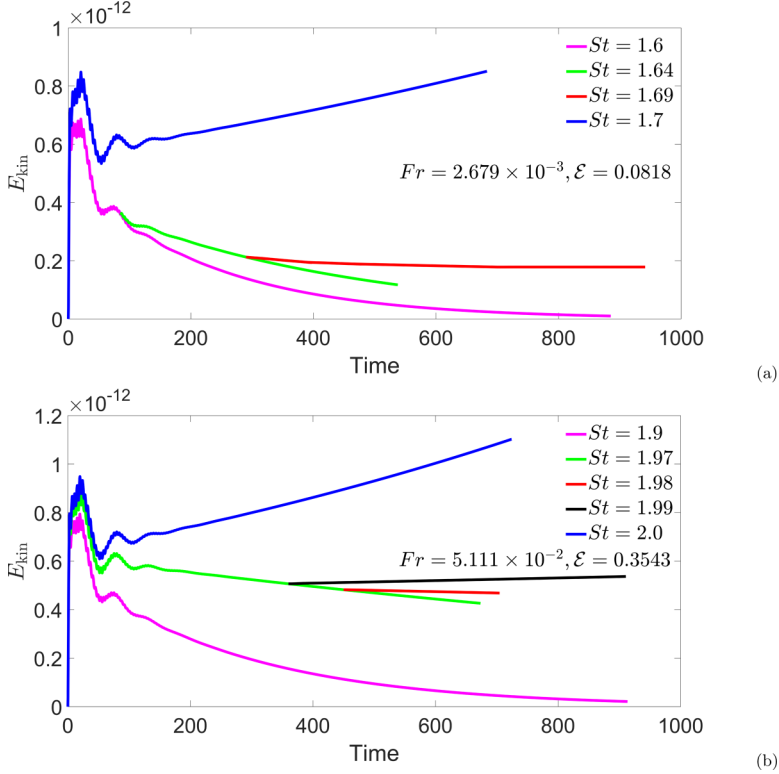


FIG. 4. The kinetic energy density E_{kin} of the numerical calculations. The two panels represent the two spheroids in which the global asymptotic solutions are obtained and tabulated in Table. I. Panel (a) shows that for the first spheroid whose shape is like Earth, the numerical critical stratification number is $St_c^{\text{num}} = 1.69$. Panel (b) shows that for the second spheroid whose shape is like Jupiter, the numerical critical stratification number is $St_c^{\text{num}} = 1.98$.

has been extensively used and validated in numerically modeling various spherical dynamo [34], ellipsoidal librating flow [35], and cylindrical precessing flow [70] problems.

When the key parameters Ek , Pr , and Fr are prescribed, the numerical onset of thermal convection in an oblate spheroidal cavity of eccentricity \mathcal{E} is located through a bisectional-type searching process. To start with, two calculations are launched with stratification numbers St respectively significantly higher and lower than the global critical stratification number St_c^{asym} that is predicted by the asymptotic theory. The two calculations are both initially static and perturbed randomly in temperature. After a burn-in stage, the convective flow should substantially get excited for the higher St case but quickly decay towards zero for the lower St case. The ensuing procedure is iterative, involving gradually adjusting the St until the convection can be marginally sustained. The iterations terminate when the numerically critical stratification number St_c^{num} converges to the second decimal. In Fig. 4, the kinetic energy density of flow, which is defined by the volumetric mean of kinetic energy,

$$E_{\text{kin}} = \frac{3}{4\pi\sqrt{1-\mathcal{E}^2}} \int_{\mathcal{D}} \frac{1}{2} |\mathbf{u}|^2 dV, \quad (72)$$

is plotted for the calculated cases inside three spheroids.

Further, snapshots are displayed in Fig. 5 showing the azimuthal velocity of convective flows and temperature isosurfaces of the three numerically critical convections. The structures of the flows are all consistent with the nonaxisymmetric quasigeostrophic (2,1,1) mode.

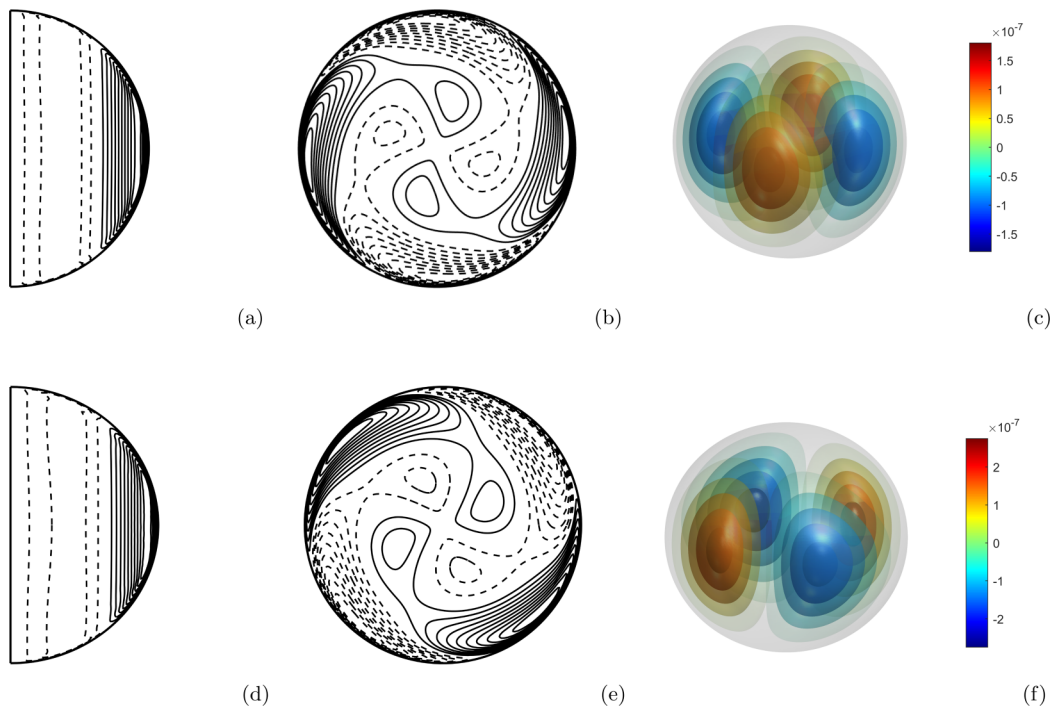


FIG. 5. Snapshots of the numerical solutions of critical convective flows in the two oblate spheroidal cavities. The dynamical parameters are $Ek = 10^{-4}$ and $Pr = 5 \times 10^{-3}$. The top and the bottom rows respectively hold the solutions in the $\mathcal{E} = 0.0818$ and $\mathcal{E} = 0.3543$ spheroids. Their stratification numbers St_c^{num} are indicated by Fig. 4. The left column of panels (a) and (d) plot the azimuthal component of flow $\hat{\phi} \cdot \mathbf{u}$ in two meridional cross-sections of the spheroids. Solid contours depict positive-valued speed and dashed contours represent negative-valued speed. The middle column of panels (b) and (e) plot the azimuthal component of flow $\hat{\phi} \cdot \mathbf{u}$ in the equatorial planes of the spheroids. Solid contours depict positive-valued speed and dashed contours represent negative-valued speed. The right column of panels (c) and (f) plot the isosurfaces of temperature Θ in the three spheroids. All panels can clearly show the three critical flows are dominated by the (2,1,1) mode.

Finally, it is ready to compare the numerical solutions and the asymptotic solutions for their onset properties. Table II demonstrates an excellent consistency between the numerical and asymptotic solutions.

V. CONCLUDING REMARKS

Coriolis force plays a predominant role in the dynamics of rapidly rotating fluids. In the three-dimensional space, the Coriolis force alters the symmetry of the Navier-Stokes equation, which fundamentally changes the topology of the dynamics [8]. It has been widely demonstrated

TABLE II. Comparison of the numerical and asymptotic solutions. A superscript “asym” denotes the result computed with the asymptotic solution. A superscript “num” suggests a numerical result.

Ek	Pr	Fr	\mathcal{E}	$(m_c, n_c, k_c)^{\text{asym}}$	$(m_c, n_c, k_c)^{\text{num}}$	St_c^{asym}	St_c^{num}	σ_c^{asym}	σ_c^{num}
10^{-4}	5×10^{-3}	2.6791×10^{-3}	0.0818	(2,1,1)	(2,1,1)	1.64	1.69	-0.1096	-0.1001
		5.1108×10^{-2}	0.3543	(2,1,1)	(2,1,1)	1.92	1.98	-0.1106	-0.1010

by many researchers that the onset of rotating convection and the weakly nonlinear properties of rotating convection are much more complicated than those in the nonrotating regime [7,71,72]. Ekman number and Prandtl number are regarded to be the key *a priori* parameters to determine the characteristics of dynamics near the onset of rotating convection.

Besides Coriolis force, the rapid rotation will also lead to the centrifugal force in the corotating frame of reference. It can flatten a rotating self-gravitating fluid body from a spherical shape to an oblate spheroidal one, which not only transforms the domain in which equations are defined but also changes relevant boundary conditions. It also directly enters Navier-Stokes equation as part of the effective gravity $\mathbf{g}_{\text{eff}} = \mathbf{g}_0 - \boldsymbol{\Omega} \times (\boldsymbol{\Omega} \times \mathbf{r})$. Another essentially important parameter to do with the dynamics of rotating convection is therefore the Froude number. In this paper, for the first time, the thermal Boussinesq convection problem is self-consistently formulated and analyzed inside a rapidly rotating oblate spheroidal cavity, taking full account of both the Coriolis force and the centrifugal force into topology analysis. Based on the assumption of the Ekman number is asymptotically small and the Prandtl number is sufficiently small, a global asymptotic solution is obtained for the thermal inertial convection problem subject to no-slip and isothermal boundary conditions. The onset of thermal instability of each inertial mode can be represented by a critical stratification number and a small shift in the half-frequency of the mode.

For the particular parameter space demonstrated in this paper, it is discovered that the critical stratification number for inertial modes generally rises with the increase of the Froude number, which means a planet that is rotating faster might require more energetic internal heating to excite and sustain thermal inertial waves. It might also suggest that if a planet's rotation is slowing down due to tidal dissipation before the planet is cooling down, abundant internal inertial waves could be induced. Although it is not straightforward to directly connect the current theory to various phenomena yet, the role that the Froude number is playing perhaps helps understand questions such as why the Moon could sustain its internal dynamics longer than Mars; why Venus has lost its active dynamo process while our Earth is having one; and why the internal MHD properties are so different between the two giant gaseous planets Jupiter and Saturn.

Choice of length scale for nondimensionalization might affect the interpretations in the above paragraph. But the key fact remains true that linear onset of rotating convection apparently depends on centrifugal effect, which has not been studied before this paper. Nonsphericity introduces another degree of freedom to the dynamics, which calls for further explorations. Next, thermal convection problems in oblate spheroidal cavities with moderate to large Prandtl number will be examined. The corresponding so-called viscous convection may bring other interesting results.

ACKNOWLEDGMENTS

This work was supported by B-type Strategic Priority Program of the Chinese Academy of Sciences (Grant No. XDB41000000); Hong Kong-Macau-Taiwan Cooperation Funding of Shanghai Committee of Science and Technology (Grant No. 19590761300); Preresearch Project on Civil Aerospace Technologies funded by China National Space Administration (Grant No. D020303); Macau Science and Technology Development Fund (Grant No. 0005/2019/A1); National Natural Science Foundation of China (Grant No. 12273092). The computation made use of the high-performance computing resources in the Core Facility for Advanced Research Computing at Shanghai Astronomical Observatory, Chinese Academy of Sciences.

APPENDIX: THE BOUNDARY LAYER SOLUTION

In the boundary layer the flow $\tilde{\mathbf{u}}$ is decomposed into the tangential component $\tilde{\mathbf{u}}_{\text{tang}}$ and the normal component $\hat{\boldsymbol{\eta}}(\hat{\boldsymbol{\eta}} \cdot \tilde{\mathbf{u}})$: $\tilde{\mathbf{u}} = \tilde{\mathbf{u}}_{\text{tang}} + \hat{\boldsymbol{\eta}}(\hat{\boldsymbol{\eta}} \cdot \tilde{\mathbf{u}})$. Substituting Eqs. (40)–(44) into Eqs. (35)–(37) yields the equation in the boundary layer,

$$i2\sigma_{mnk}\tilde{\mathbf{u}} + 2\hat{\mathbf{z}} \times \tilde{\mathbf{u}} + \hat{\boldsymbol{\eta}}(\hat{\boldsymbol{\eta}} \cdot \nabla \tilde{p}) = \frac{\text{Ek}}{1 - \mathcal{E}^2(1 - \tau^2)} \frac{\partial^2 \tilde{\mathbf{u}}}{\partial \eta^2}, \quad (\text{A1})$$

where the small terms, such as $\partial^2 \tilde{\mathbf{u}} / \partial \tau^2$, $\partial^2 \tilde{\mathbf{u}} / \partial \phi^2$ and the tangential part of $\nabla \tilde{p}$, have been neglected. Applying $\hat{\boldsymbol{\eta}} \times$ and $\hat{\boldsymbol{\eta}} \times \hat{\boldsymbol{\eta}} \times$ to Eq. (A1) produces the two second-order differential equations,

$$\left(\text{Ek} \frac{\partial^2}{\partial \eta^2} - i2\sigma_{mnk} h^2 \right) \hat{\boldsymbol{\eta}} \times \tilde{\mathbf{u}}_{\text{tang}} = -2\tau h \tilde{\mathbf{u}}_{\text{tang}}, \quad (\text{A2})$$

$$\left(\text{Ek} \frac{\partial^2}{\partial \eta^2} - i2\sigma_{mnk} h^2 \right) \tilde{\mathbf{u}}_{\text{tang}} = 2\tau h (\hat{\boldsymbol{\eta}} \times \tilde{\mathbf{u}}_{\text{tang}}), \quad (\text{A3})$$

where $h = \sqrt{1 - \mathcal{E}^2(1 - \tau^2)}$ and $|\hat{\boldsymbol{\eta}} \cdot \tilde{\mathbf{u}}| \ll |\tilde{\mathbf{u}}_{\text{tang}}|$ is assumed. The combination of Eq. (A2) and Eq. (A3) result in a fourth-order differential equation,

$$\left[\left(\frac{\partial^2}{\partial \xi^2} - i2\sigma_{mnk} h^2 \right)^2 + 4\tau^2 h^2 \right] \tilde{\mathbf{u}}_{\text{tang}} = \mathbf{0}, \quad (\text{A4})$$

where the boundary variable $\xi = (\sqrt{1 - \mathcal{E}^2} - \eta) / \sqrt{\text{Ek}}$, subject to the four boundary conditions,

$$(\tilde{\mathbf{u}}_{\text{tang}})_{\xi=0} = -[\mathbf{u}_{mnk}]_{\eta=\sqrt{1-\mathcal{E}^2}}, \quad (\text{A5})$$

$$\left(\frac{\partial^2 \tilde{\mathbf{u}}_{\text{tang}}}{\partial \xi^2} \right)_{\xi=0} = -[i2\sigma_{mnk} h^2 \mathbf{u}_{mnk} + 2\tau h \hat{\boldsymbol{\eta}} \times \mathbf{u}_{mnk}]_{\eta=\sqrt{1-\mathcal{E}^2}}, \quad (\text{A6})$$

$$(\tilde{\mathbf{u}}_{\text{tang}})_{\xi \rightarrow \infty} = \mathbf{0}, \quad (\text{A7})$$

$$\left(\frac{\partial^2 \tilde{\mathbf{u}}_{\text{tang}}}{\partial \xi^2} \right)_{\xi \rightarrow \infty} = \mathbf{0}. \quad (\text{A8})$$

Among the four boundary conditions, Eq. (A5) is required by the no-slip boundary condition that must be obeyed by the sum of $\tilde{\mathbf{u}}_{\text{tang}}$ and the mainstream \mathbf{u}_{mnk} ; Eq. (A6) is derived from Eq. (A3); Eqs. (A7) and (A8) result from the definition of a boundary layer. The solution of Eq. (A4) satisfying the four boundary conditions is

$$\begin{aligned} \tilde{\mathbf{u}}_{\text{tang}} = & -\frac{1}{2} [\mathbf{u}_{mnk} - i\hat{\boldsymbol{\eta}} \times \mathbf{u}_{mnk}]_{\eta=\sqrt{1-\mathcal{E}^2}} e^{\gamma_{mnk}^+ \xi} \\ & -\frac{1}{2} [\mathbf{u}_{mnk} + i\hat{\boldsymbol{\eta}} \times \mathbf{u}_{mnk}]_{\eta=\sqrt{1-\mathcal{E}^2}} e^{\gamma_{mnk}^- \xi}, \end{aligned} \quad (\text{A9})$$

where the two parameters are defined as

$$\gamma_{mnk}^+ = -\left(1 + i \frac{\sigma_{mnk} h^2 + \tau h}{|\sigma_{mnk} h^2 + \tau h|} \right) \sqrt{|\sigma_{mnk} h^2 + \tau h|}, \quad (\text{A10})$$

$$\gamma_{mnk}^- = -\left(1 + i \frac{\sigma_{mnk} h^2 - \tau h}{|\sigma_{mnk} h^2 - \tau h|} \right) \sqrt{|\sigma_{mnk} h^2 - \tau h|}. \quad (\text{A11})$$

Note that the characteristic thickness of boundary layer, as estimated from Eqs. (A9)–(A11), is of the order $(\text{Ek}/\sigma_{mnk})^{1/2}$, thicker than a typical Ekman layer. Although the boundary layer solution breaks down at critical latitudes [73],

$$\tau = \pm \sigma_{mnk} \frac{\sqrt{1 - \mathcal{E}^2}}{\sqrt{1 - \sigma_{mnk}^2 \mathcal{E}^2}}, \quad (\text{A12})$$

it is assumed that the effects of the breakdown on the asymptotic solution is negligible for arbitrarily small but nonzero Ek, which was proved in sphere [15,62].

The radial component $\hat{\boldsymbol{\eta}} \cdot \tilde{\mathbf{u}}$ at the outer edge of the boundary layer is related to the tangential boundary flow $\tilde{\mathbf{u}}_{\text{tang}}$ via the equation of mass conservation $\nabla \cdot \tilde{\mathbf{u}} = 0$ in the boundary layer,

$$\frac{\partial}{\partial \xi} (h \hat{\boldsymbol{\eta}} \cdot \tilde{\mathbf{u}}) = \sqrt{\text{Ek}} \left[\frac{\partial}{\partial \tau} (h \sqrt{1 - \tau^2} \hat{\boldsymbol{\tau}} \cdot \tilde{\mathbf{u}}_{\text{tang}}) + \frac{h^2}{\sqrt{1 - \tau^2}} \frac{\partial}{\partial \phi} (\hat{\boldsymbol{\phi}} \cdot \tilde{\mathbf{u}}_{\text{tang}}) \right]. \quad (\text{A13})$$

To simplify the mathematical expression, we introduce the following notations:

$$P_{mnk}(\tau) = [p_{mnk}]_{\eta=\sqrt{1-\varepsilon^2}} e^{-im\phi}, \quad (\text{A14})$$

$$V_{mnk}^\tau(\tau) = i[\hat{\boldsymbol{\tau}} \cdot \mathbf{u}_{mnk}]_{\eta=\sqrt{1-\varepsilon^2}} e^{-im\phi}, \quad (\text{A15})$$

$$V_{mnk}^\phi(\tau) = [\hat{\boldsymbol{\phi}} \cdot \mathbf{u}_{mnk}]_{\eta=\sqrt{1-\varepsilon^2}} e^{-im\phi}, \quad (\text{A16})$$

where P_{mnk} , V_{mnk}^τ , and V_{mnk}^ϕ are just real functions of τ . It is therefore convenient to separate the variables ξ , τ , and ϕ in Eq. (A13) by writing

$$\begin{aligned} & \frac{\partial}{\partial \tau} (h\sqrt{1-\tau^2} \hat{\boldsymbol{\tau}} \cdot \tilde{\mathbf{u}}_{\text{tang}}) + \frac{h^2}{\sqrt{1-\tau^2}} \frac{\partial}{\partial \phi} (\hat{\boldsymbol{\phi}} \cdot \tilde{\mathbf{u}}_{\text{tang}}) = \frac{i}{2} e^{im\phi} \\ & \times \left\{ \frac{\partial}{\partial \tau} [h\sqrt{1-\tau^2} (V_{mnk}^\tau + V_{mnk}^\phi) e^{\gamma_{mnk}^+ \xi}] - \frac{mh^2}{\sqrt{1-\tau^2}} (V_{mnk}^\tau + V_{mnk}^\phi) e^{\gamma_{mnk}^+ \xi} \right. \\ & \left. + \frac{\partial}{\partial \tau} [h\sqrt{1-\tau^2} (V_{mnk}^\tau - V_{mnk}^\phi) e^{\gamma_{mnk}^- \xi}] + \frac{mh^2}{\sqrt{1-\tau^2}} (V_{mnk}^\tau - V_{mnk}^\phi) e^{\gamma_{mnk}^- \xi} \right\}. \quad (\text{A17}) \end{aligned}$$

Integration of Eq. (A13) over ξ yields the normal flux $\hat{\boldsymbol{\eta}} \cdot \tilde{\mathbf{u}}$ at the top of the boundary layer

$$\begin{aligned} (\hat{\boldsymbol{\eta}} \cdot \tilde{\mathbf{u}})_{\xi \rightarrow \infty} &= \frac{\sqrt{\text{Ek}}}{h} \int_0^\infty \left[\frac{\partial}{\partial \tau} (h\sqrt{1-\tau^2} \hat{\boldsymbol{\tau}} \cdot \tilde{\mathbf{u}}_{\text{tang}}) + \frac{h^2}{\sqrt{1-\tau^2}} \frac{\partial}{\partial \phi} (\hat{\boldsymbol{\phi}} \cdot \tilde{\mathbf{u}}_{\text{tang}}) \right] d\xi \\ &= -\frac{i\sqrt{\text{Ek}}}{2h} e^{im\phi} \left\{ \frac{d}{d\tau} \left[\frac{h\sqrt{1-\tau^2}}{\gamma_{mnk}^+} (V_{mnk}^\tau + V_{mnk}^\phi) \right] - \frac{mh^2}{\gamma_{mnk}^+ \sqrt{1-\tau^2}} (V_{mnk}^\tau + V_{mnk}^\phi) \right. \\ & \left. + \frac{d}{d\tau} \left[\frac{h\sqrt{1-\tau^2}}{\gamma_{mnk}^-} (V_{mnk}^\tau - V_{mnk}^\phi) \right] + \frac{mh^2}{\gamma_{mnk}^- \sqrt{1-\tau^2}} (V_{mnk}^\tau - V_{mnk}^\phi) \right\}. \quad (\text{A18}) \end{aligned}$$

-
- [1] D. Gubbins, T. G. Masters, and J. A. Jacobs, Thermal evolution of the Earth's core, *Geophys. J. Int.* **59**, 57 (1979).
- [2] S. Müller, R. Helled, and A. Cumming, The challenge of forming a fuzzy core in Jupiter, *Astron. Astrophys.* **638**, A121 (2020).
- [3] M. Bouffard, G. Choblet, S. Labrosse, and J. Wicht, Chemical convection and stratification in the Earth's outer core, *Front. Earth Sci.* **7**, 99 (2019).
- [4] C. A. Jones, Planetary magnetic fields and fluid dynamos, *Annu. Rev. Fluid Mech.* **43**, 583 (2011).
- [5] N. Schaeffer, D. Jault, H.-C. Nataf, and A. Fournier, Turbulent geodynamo simulations: A leap towards Earth's core, *Geophys. J. Int.* **211**, 1 (2017).
- [6] J. Wicht and S. Sanchez, Advances in geodynamo modelling, *Geophys. Astrophys. Fluid Dyn.* **113**, 2 (2019).
- [7] K. Zhang and G. Schubert, Magnetohydrodynamics in rapidly rotating spherical systems, *Annu. Rev. Fluid Mech.* **32**, 409 (2000).
- [8] J. Sánchez Umbría and M. Net, Continuation of double Hopf points in thermal convection of rotating fluid spheres, *SIAM J. Appl. Dyn. Syst.* **20**, 208 (2021).
- [9] S. Chandrasekhar, *Hydrodynamic and Hydromagnetic Stability* (Clarendon Press, Oxford, UK, 1962).
- [10] P. H. Roberts, On the thermal instability of a rotating-fluid sphere containing heat sources, *Phil. Trans. R. Soc. Lond. A* **263**, 93 (1968).
- [11] F. Busse, Thermal instabilities in rapidly rotating systems, *J. Fluid Mech.* **44**, 441 (1970).
- [12] A. M. Soward, On the finite amplitude thermal instability of a rapidly rotating fluid sphere, *Geophys. Astrophys. Fluid Dyn.* **9**, 19 (1977).

- [13] J.-I. Yano, Asymptotic theory of thermal convection in rapidly rotating systems, *J. Fluid Mech.* **243**, 103 (1992).
- [14] K. Zhang, On coupling between the Poincaré equation and the heat equation, *J. Fluid Mech.* **268**, 211 (1994).
- [15] K. Zhang, On coupling between the Poincaré equation and the heat equation: Nonslip boundary condition, *J. Fluid Mech.* **284**, 239 (1995).
- [16] C. A. Jones, A. W. Soward, and A. I. Mussa, The onset of thermal convection in a rapidly rotating sphere, *J. Fluid Mech.* **405**, 157 (2000).
- [17] K. Zhang and X. Liao, A new asymptotic method for the analysis of convection in a rapidly rotating sphere, *J. Fluid Mech.* **518**, 319 (2004).
- [18] E. Dormy, A. M. Soward, C. A. Jones, D. Jault, and P. Cardin, The onset of thermal convection in rotating spherical shells, *J. Fluid Mech.* **501**, 43 (2004).
- [19] P. Olson, 8.01-core dynamics: An introduction and overview, in *Treatise on Geophysics*, 2nd ed., edited by G. Schubert (Elsevier, Oxford, UK, 2015), pp. 1–25.
- [20] F. Busse, A simple model of convection in the Jovian atmosphere, *Icarus* **29**, 255 (1976).
- [21] A. P. Ingersoll and D. Pollard, Motion in the interiors and atmospheres of Jupiter and Saturn: Scale analysis, anelastic equations, barotropic stability criterion, *Icarus* **52**, 62 (1982).
- [22] K. Zhang, Spiralling columnar convection in rapidly rotating spherical fluid shells, *J. Fluid Mech.* **236**, 535 (1992).
- [23] M. Heimpel, J. Aurnou, and J. Wicht, Simulation of equatorial and high-latitude jets on Jupiter in a deep convection model, *Nature (London)* **438**, 193 (2005).
- [24] T. Gastine, J. Wicht, and J. Aubert, Scaling regimes in spherical shell rotating convection, *J. Fluid Mech.* **808**, 690 (2016).
- [25] S. Maffei, A. Jackson, and P. W. Livermore, Characterization of columnar inertial modes in rapidly rotating spheres and spheroids, *Proc. R. Soc. A.* **473**, 20170181 (2017).
- [26] C. Guervilly, P. Cardin, and N. Schaeffer, Turbulent convective length scale in planetary cores, *Nature (London)* **570**, 368 (2019).
- [27] Y. Lin and A. Jackson, Large-scale vortices and zonal flows in spherical rotating convection, *J. Fluid Mech.* **912**, A46 (2020).
- [28] S. Chandrasekhar, Ellipsoidal figures of equilibrium-an historical account, *Comm. Pure Appl. Math.* **20**, 251 (1967).
- [29] H. Lamb, *Hydrodynamics*, Dover Books on Physics (Dover Publications, Oxford, UK, 1945).
- [30] W. B. Hubbard, G. Schubert, D. Kong, and K. Zhang, On the convergence of the theory of figures, *Icarus* **242**, 138 (2014).
- [31] N. Nettelmann, N. Movshovitz, D. Ni *et al.*, Theory of figures to the seventh order and the interiors of Jupiter and Saturn, *Planet. Sci. J.* **2**, 241 (2021).
- [32] A. Jackson, A. Sheyko, P. Marti *et al.*, A spherical shell numerical dynamo benchmark with pseudo-vacuum magnetic boundary conditions, *Geophys. J. Int.* **196**, 712 (2014).
- [33] H. Matsui, E. Heien, J. Aubert *et al.*, Performance benchmarks for a next generation numerical dynamo model, *Geochem. Geophys. Geosyst.* **17**, 1586 (2016).
- [34] K. H. Chan, K. Zhang, L. Li, and X. Liao, A new generation of convection-driven spherical dynamos using EBE finite element method, *Phys. Earth Planet. Inter.* **163**, 251 (2007).
- [35] K. H. Chan, Y. He, K. Zhang, and J. Zou, A finite element analysis on fluid motion in librating triaxial ellipsoids, *Numer. Methods Partial Differ. Equat.* **30**, 1518 (2014).
- [36] E. H. von Zeipel, The radiative equilibrium of a rotating system of gaseous masses, *Mon. Not. R. Astron. Soc.* **84**, 665 (1924).
- [37] A. Eddington, Circulating currents in rotating stars, *Observatory* **48**, 73 (1925).
- [38] J. H. Jeans, On a theorem of v. zeipel on radiative equilibrium, *Mon. Not. R. Astron. Soc.* **85**, 526 (1925).
- [39] M. Schwarzschild, On stellar rotation, *Astrophys. J.* **95**, 441 (1942).
- [40] E. J. Öpik, Rotational currents, *Mon. Not. R. Astron. Soc.* **111**, 278 (1951).
- [41] F. Busse, Do eddington-sweet circulations exist? *Geophys. Astrophys. Fluid Dyn.* **17**, 215 (1981).

- [42] J.-L. Tassoul and M. Tassoul, Meridional circulation in rotating stars. I. A boundary layer analysis of mean steady motions in early-type stars, *Astrophys. J. Suppl. Series* **49**, 317 (1982).
- [43] H. C. Spruit and E. Knobloch, Baroclinic instability in stars, *Astron. Astrophys.* **132**, 89 (1984).
- [44] U. Schneider, Baroclinic zonal currents in rotating stars, *Astron. Astrophys.* **238**, 142 (1990).
- [45] J. P. Zahn, Circulation and turbulence in rotating stars, *Astron. Astrophys.* **265**, 115 (1992).
- [46] M. Rieutord, The dynamics of the radiative envelope of rapidly rotating stars, I. A spherical boussinesq model, *Astron. Astrophys.* **451**, 1025 (2006).
- [47] R. D. Simitiev and F. H. Busse, Baroclinically-driven flows and dynamo action in rotating spherical fluid shells, *Geophys. Astrophys. Fluid Dyn.* **111**, 369 (2017).
- [48] D. Kong, Rapidly rotating self-gravitating Boussinesq fluid: A nonspherical model of motionless stable stratification, *Phys. Rev. Fluids* **7**, 074803 (2022).
- [49] A. Meilland, P. Stee, M. Vannier *et al.*, First direct detection of a Keplerian rotating disk around the be star α Arae using Amber/VLTI, *Astron. Astrophys.* **464**, 59 (2007).
- [50] P. Kervella, A. Domiciano de Souza, S. Kanaan *et al.*, The environment of the fast rotating star Achernar, II. Thermal infrared interferometry with VLTI/MIDI, *Astron. Astrophys.* **493**, L53 (2009).
- [51] A. Maeder, C. Georgy, and D. Meynet, Convective envelopes in rotating OB stars, *Astron. Astrophys.* **479**, L37 (2008).
- [52] S. M. Wahl, W. B. Hubbard, B. Militzer *et al.*, Comparing Jupiter interior structure models to Juno gravity measurements and the role of a dilute core, *Geophys. Res. Lett.* **44**, 4649 (2017).
- [53] L. Iess, W. M. Folkner, D. Durante *et al.*, Measurement of Jupiter's asymmetric gravity field, *Nature (London)* **555**, 220 (2018).
- [54] D. Kong, K. Zhang, G. Schubert, and J. D. Anderson, Origin of Jupiter's cloud-level zonal winds remains a puzzle even after Juno, *Proc. Natl. Acad. Sci. USA* **115**, 8499 (2018).
- [55] L. Iess, B. Militzer, Y. Kaspi *et al.*, Measurement and implications of Saturn's gravity field and ring mass, *Science* **364**, eaat2965 (2019).
- [56] D. Kong, K. Zhang, and G. Schubert, A fully self-consistent multi-layered model of Jupiter, *Astrophys. J.* **826**, 127 (2016).
- [57] D. Kong, K. Zhang, and G. Schubert, Depth of the dynamo region and zonal circulation of the molecular layer in Saturn inferred from its equatorially symmetric gravitational field, *Month. Not. Roy. Astron. Soc.* **488**, 5633 (2019).
- [58] D. Ni, Understanding Saturn's interior from the Cassini grand finale gravity measurements, *Astron. Astrophys.* **639**, A10 (2020).
- [59] K. Zhang, X. Liao, and P. Earnshaw, On inertial waves and oscillations in a rapidly rotating spheroid, *J. Fluid Mech.* **504**, 1 (1999).
- [60] K. Zhang, K. Lam, and D. Kong, Asymptotic theory for torsional convection in rotating fluid spheres, *J. Fluid Mech.* **813**, R2 (2017).
- [61] K.-K. Zhang and F. H. Busse, On the onset of convection in rotating spherical shells, *Geophys. Astrophys. Fluid Dynam.* **39**, 119 (1987).
- [62] K. Zhang, X. Liao, and F. H. Busse, Asymptotic solutions of convection in rapidly rotating nonslip spheres, *J. Fluid Mech.* **578**, 371 (2007).
- [63] K. Zhang and X. Liao, *Theory and Modeling of Rotating Fluids: Convection, Inertial Waves and Precession* (Cambridge University Press, Cambridge, UK, 2017).
- [64] C. Flammer, *Spheroidal Wave Functions* (Stanford University Press, Stanford, CA, 1957).
- [65] M. Abramowitz and I. A. Stegun, *Handbook of Mathematical Functions with Formulas, Graphs, and Mathematical Tables* (U.S. Government Printing Office, Washington, D.C., 1964) Chap. 21.
- [66] K. Chan, K. Zhang, and X. Liao, An EBE finite element method for simulating nonlinear flows in rotating spheroidal cavities, *Int. J. Numer. Methods Fluids* **63**, 395 (2010).
- [67] U. M. Ascher and L. R. Petzold, *Computer Methods for Ordinary Differential Equations and Differential-Algebraic Equations* (SIAM, Philadelphia, PA, 1998).
- [68] V. John, *Finite Element Spaces for Linear Saddle Point Problems* (Springer, Cham, 2016).
- [69] G. L. G. Sleijpen and D. R. Fokkema, Bicgstab(l) for linear equations involving unsymmetric matrices with complex spectrum, *Electr. Trans. Numer. Anal.* **1**, 11 (1993).

- [70] D. Kong, X. Liao, and K. Zhang, The sidewall-localized mode in a resonant precessing cylinder, [Phys. Fluids](#) **26**, 051703 (2014).
- [71] E. J. Kaplan, N. Schaeffer, J. Vidal, and P. Cardin, Subcritical Thermal Convection of Liquid Metals in a Rapidly Rotating Sphere, [Phys. Rev. Lett.](#) **119**, 094501 (2017).
- [72] D. Kong, K. Zhang, K. Lam, and A. P. Willis, Axially symmetric and latitudinally propagating nonlinear patterns in rotating spherical convection, [Phys. Rev. E](#) **98**, 031101(R) (2018).
- [73] P. H. Roberts, On the thermal instability of a highly rotating fluid sphere, [Astrophys. J.](#) **141**, 240 (1965).